Draft version January 13, 2011
Preprint typeset using LaTeX style emulateapj v. 08/22/09

THE COSMOGRID SIMULATION: STATISTICAL PROPERTIES OF SMALL DARK MATTER HALOS

TOMOAKI Ishiyama[1], JUNICHIRO Makino[1], SIMON Portegies Zwart[2], DEREK Groen[3], KEIGO Nitadori[4], STEVEN Rieder[2,5], CEES de Laat[5], STEPHEN McMillan[6], KEI Hiraki[7], and STEFAN Harfst[8]

Draft version January 13, 2011

ABSTRACT

We present the results of the "Cosmogrid" cosmological N-body simulation suites based on the concordance LCDM model. The Cosmogrid simulation was performed in a 30Mpc box with 2048^3 particles. The mass of each particle is $1.28 \times 10^5 M_\odot$, which is sufficient to resolve ultra-faint dwarfs. We found that the halo mass function shows good agreement with the Sheth & Tormen (1999) fitting function down to $\sim 10^7 M_\odot$. We have analyzed the spherically averaged density profiles of the three most massive halos which are of galaxy group size and contain at least 170 million particles. The slopes of these density profiles become shallower than -1 at the inner most radius. We also find a clear correlation of halo concentration with mass. The mass dependence of the concentration parameter cannot be expressed by a single power law, however a simple model based on the Press-Schechter theory gives reasonable agreement with this dependence. The spin parameter does not show a correlation with the halo mass. The probability distribution functions for both concentration and spin are well fitted by the log-normal distribution for halos with the masses larger than $\sim 10^8 M_\odot$.

Subject headings: cosmology: theory —galaxies: dwarf —methods: numerical —dark matter

1. INTRODUCTION

According to the present standard LCDM model, the Universe is thought to be composed primarily of cold dark matter (CDM) and dark energy (White & Rees 1978; Peacock 1999). Structure formation of the Universe proceeds hierarchically in this model. Smaller-scale structures collapse first, and then merge into larger-scale structures.

There is serious discrepancy between the distribution of subhalos in galaxy-sized halos obtained by numerical simulations and the observed number of dwarf galaxies in the Local Group (Klypin et al. 1999; Moore et al. 1999a). This "missing dwarf problem" is still considered to be one of the most serious problem in the CDM paradigm (e.g. Kroupa et al. 2010). In order to understand the origin of this discrepancy, it is necessary to perform high-resolution cosmological N-body simulations and obtain unbiased sample of galaxy-sized halos with resolution high enough to obtain reliable statistics of subhalos since the subhalo abundance shows large halo-to-halo variations (Ishiyama et al. 2009b).

Cosmological N-body simulations have been widely used to study the nonlinear structure formation of the Universe and have been an important tool for a better understanding of our Universe. In order to study the spatial correlation of galaxies, the first cosmological N-body simulations were performed in the 1970s using approximately 1000 particles (e.g. Miyoshi & Kihara 1975; Fall 1978; Aarseth et al. 1979; Efstathiou 1979). Since then, the development of better simulation algorithms and improvements in the performance of computers allow us to use much larger numbers of particles and have drastically increased the resolution of cosmological simulations.

Today, it is not uncommon that the number of particles exceeds 10^9 in high resolution simulations. In these works, the size of the simulation volumes is typically $[O(\mathrm{Gpc})]^3$ and populations of galaxy clusters, gravitational lensing, and the baryon acoustic oscillation are studied (e.g. Evrard et al. 2002; Wambsganss et al. 2004; Teyssier et al. 2009; Kim et al. 2009; Crocce et al. 2010). The simulation results are also used to construct mock halo catalogues for next generation large volume surveys. Others use simulations of $[O(100\mathrm{Mpc})]^3$ volumes to study the internal properties of galaxy-sized dark matter halos, their formation, evolution, and statistical properties (e.g. Springel et al. 2005; Klypin et al. 2010; White et al. 2010).

Using the results of high-resolution simulations of small-scale structures, we can study the fine structures of galactic halos, the distribution of subhalos, their structures, and their dependence on the nature of dark matter. This information has a strong impact on the indirect search for dark matter since gamma-ray flux by self-annihilation is proportional to local density if we consider neutralino as the candidate of dark matter. Thus, we can restrict the nature of dark matter using the results of high-resolution simulations of small-scale structures and indirect searches of dark matter. In addition, galaxies are considered to form in dark matter halos with a mass larger than a critical value (Strigari et al. 2008; Li et al. 2009; Macciò et al. 2009; Okamoto & Frenk 2009). The structures of smallest halos which can host galaxies is

[1] National Astronomical Observatory of Japan, Mitaka, Tokyo 181-8588, Japan ; ishiyama@cfca.jp
[2] Sterrewacht Leiden, Leiden University, P.O. Box 9513, 2300 RA Leiden, The Netherlands
[3] Centre for Computational Science, Department of Chemistry, University College London, 20 Gordon Street, London, WC1H 0AJ, UK
[4] RIKEN, 2-1, Hirosawa, Wako, Saitama 351-0198, Japan
[5] Section System and Network Engineering, University of Amsterdam, Amsterdam, The Netherlands
[6] Department of Physics, Drexel University, Philadelphia, PA 19104, USA
[7] Department of Creative Informatics, Graduate School of Information Science and Technology the University of Tokyo, Japan
[8] Center for Astronomy and Astrophysics, Technical University Berlin, Hardenbergstr. 36, 10623 Berlin, Germany

important for the understanding of the galaxy formation processes.

The simulation of smaller-scale structures of dark matter halos is not a trivial task since a very wide dynamic ranges of space, mass, and time must be covered. In particular, the number of time steps of such simulations is significantly larger than that of larger-scale simulations since the dynamical time scale is proportional to $1.0/\sqrt{G\bar{\rho}}$, where $\bar{\rho}$ is the local density. Structures of smaller-scales form earlier, and thus have higher densities, therefore, simulations of smaller scales are computationally more expensive.

Recently, simulations with galactic halos of very high resolution have been performed (Diemand et al. 2008; Springel et al. 2008; Stadel et al. 2009). These works used the re-simulation method, where one selects one or a few halos at $z = 0$ from a simulation which covers a large volume [typically a cube of size O(100Mpc)] with a relatively low-resolution. The corresponding regions of these halos are then identified in the initial particle distribution, and the particles in these regions are replaced by a larger number of smaller particles. After this is done, the entire volume is simulated to $z = 0$ again.

With this re-simulation method, we can resolve the structures of selected halos with extremely high resolution (Diemand et al. 2008; Springel et al. 2008; Stadel et al. 2009). However, this method cannot be used for the study of halo-to-halo variations. Different halos are born in different environments and grow differently. The difference in the environment and growth history must be the cause of halo-to-halo variations. Therefore, in order to study variations, we need a bias-free set of a large number of halos. Clearly one cannot obtain a large number of halos with re-simulation method in practical time.

In principle, one can improve the statistics by increasing the number of halos selected for re-simulations. In order to avoid the selection bias, we need to apply random, bias-free selection, and the most reliable bias-free selection is to select all halos, in other words, to simulate the entire simulation box with uniformly high mass resolution. Ishiyama et al. (2009b) performed the first bias-free high resolution simulation of small-scale structures. They analyzed the statistics of the subhalo abundance using the complete set of halos in the simulation box. The number of particles was 1600^3 in a 46.5Mpc cubic box and the mass of a particle was $10^6 M_\odot$. The subhalo abundance showed large halo-to-halo variations [see also Ishiyama et al. (2008); Boylan-Kolchin et al. (2010)]. The concentration parameter and the radius at the moment of the maximum expansion showed fairly tight correlation with the subhalo abundance. Halos formed earlier have smaller number of subhalos at present. This correlation suggests that the difference in the formation history is the origin of the variation of the subhalo abundance [see also Gao et al. (2004); van den Bosch et al. (2005); Zentner et al. (2005)].

The Millennium-II simulation (Boylan-Kolchin et al. 2009) used a 137Mpc cubic box and the particle mass of $\sim 9.45 \times 10^6 M_\odot$. Its result is suitable for the analysis of the statistics of galaxy-sized dark matter halos, because the number of halos is larger than that of Ishiyama et al. (2009b). However, due to the lack of the mass resolution, it cannot be used to study the statistics of dwarf-galaxy-sized halos and the statistics of subhalos with the size larger than faint dwarf galaxy.

In this paper, we describe the first result of our Cosmogrid simulation. We simulated the evolution of halos in a 30Mpc cubic box using 2048^3 particles. The mass of one particle is $1.28 \times 10^5 M_\odot$. The resolution reaches down to ultra-faint dwarf-galaxy-sized halos ($\sim 10^7 M_\odot$) and is more than 8 times better than that of our previous simulation (Ishiyama et al. 2009b). We focus on the halo mass function with the mass down to $10^7 M_\odot$, the structures of most massive halos, and statistics of the internal properties of dwarf-galaxy-sized halos. We describe our initial conditions and numerical settings in Section 2, and results in Section 3. We discuss and summarize our results in Section 4.

2. INITIAL CONDITIONS AND NUMERICAL METHOD

The cosmological parameters adopted are based on the concordance LCDM cosmological model ($\Omega_0 = 0.3$, $\lambda_0 = 0.7$, $h = 0.7$, $\sigma_8 = 0.8$, $n = 1.0$). These values are the same as those used in our previous simulation (Ishiyama et al. 2009b). We used a periodic cube of the comoving size of 30Mpc. The number of particles for the largest run is 2048^3 which corresponds to a mass resolution of $1.28 \times 10^5 M_\odot$. To generate the initial particle distributions, we used the MPGRAFIC package (Prunet et al. 2008), which is a parallelized variation of the GRAFIC package (Bertschinger 2001). The initial redshift was 65.

In order to investigate the effect of the mass and spatial resolution, we performed two simulations with lower resolution. We generated the initial conditions for these low-resolution runs (CG1024 and CG512) by replacing eight or 64 particles in the high-resolution initial condition (CG2048) with a single particle eight or 64 times more massive. In order to study the effect of cosmological parameters, we performed an additional simulation with cosmological parameters close to recent observational values [$\Omega_0 = 0.27$, $\lambda_0 = 0.73$, $h = 0.7$, $\sigma_8 = 0.8$, $n = 0.96$, Spergel et al. (2007); Komatsu et al. (2009)]. In table 1, we summarize parameters used in our simulations.

We used a leapfrog integrator with shared and adaptive time steps. The step size was determined as $\min(2.0\sqrt{\varepsilon/|\vec{a}_i|}, 2.0\varepsilon/|\vec{v}_i|)$ (minimum of these two values for all particles). The gravitational plummer softening length ε was 175pc at $z = 0$. The softening was constant in comoving coordinates from $z = 65$ (initial condition) to $z = 10$. From $z = 10$ to $z = 0$, it was constant in physical coordinates. This procedure is similar to that used in Kawai et al. (2004).

For the largest simulation, we used four supercomputers. Three of them are Cray XT4 machines at the Center for Computational Astrophysics of National Astronomical Observatory of Japan, the Edinburgh Parallel Computing Center in Edinburgh (United Kingdom) and IT Center for Science in Espoo (Finland). The fourth machine is an IBM pSeries 575 at SARA in Amsterdam (the Netherlands). Part of the calculation was done in a "grid" computing environment, in which we used more than one machine simultaneously for one run (Portegies Zwart et al. 2010).

For the time integration we used the GreeM code

Table 1
Run parameters. Here, N, L, ε, and m are the total number of particles, the box length, the softening length, the mass resolution. The cosmological parameters are $\Omega_0 = 0.3$, $\lambda_0 = 0.7$, $h = 0.7$, $\sigma_8 = 0.8$, $n = 1.0$ for (a), and $\Omega_0 = 0.27$, $\lambda_0 = 0.73$, $h = 0.7$, $\sigma_8 = 0.8$, $n = 0.96$ for (b).

Name	N	L(Mpc)	ε(pc)	$m(\mathrm{M}_\odot)$	Cosmology
CG2048	2048^3	30.0	175	1.28×10^5	a
CG1024	1024^3	30.0	350	1.03×10^6	a
CG512	512^3	30.0	700	8.21×10^6	a
CG512WMAP	512^3	30.0	700	7.39×10^6	b
IFM2009 (Ishiyama et al. 2009b)	1600^3	46.5	700	1.00×10^6	a

Table 2
Global parameters of three most massive group sized halos at $z = 0$. Here, M, N, $R_{\rm vir}$, $R_{\rm vmax}$, and $V_{\rm max}$ are the mass, the number of particles, the virial radius in which the spherical overdensity is 101 times the critical value, the radius where the rotation velocity is maximum, and the maximum rotation velocity, respectively.

Name	Run	$M(10^{13}M_\odot)$	N	$R_{\rm vir}$(kpc)	$R_{\rm vmax}$(kpc)	$V_{\rm max}$(km/s)
GP1	CG2048	5.24	408499843	969	200	596
	CG1024	5.19	50632942	966	186	589
	CG512	5.22	6361253	968	184	596
GP2	CG2048	3.58	279382586	854	305	476
	CG1024	3.57	34836692	853	279	472
	CG512	3.57	4347651	852	294	475
GP3	CG2048	2.25	175752770	731	178	434
	CG1024	2.26	22072073	732	187	431
	CG512	2.25	2746874	731	192	434

(Ishiyama et al. 2009a) for single supercomputer runs and the SUSHI code (Groen et al. 2011) for multi-supercomputer runs. The GreeM code is a massively parallel TreePM code based on the parallel TreePM code of Yoshikawa & Fukushige (2005) for large cosmological N-body simulations. The long range forces are calculated by the PM method (Hockney & Eastwood 1981), and the short range forces are calculated by the Barnes Hut Tree method (Barnes & Hut 1986). Yoshikawa & Fukushige (2005) used a 1-D slab decomposition, but in GreeM we use a 3-D multi-section decomposition (Makino 2004) to improve its scalability. In addition, the decomposition is based on CPU time measurement, so that near ideal load balance is archived. The SUSHI code is an extension of the GreeM code which can run concurrently on multiple supercomputers. It uses the MPWide communication library (Groen et al. 2010) to facilitate message passing between distributed supercomputers. We used 512^3 PM grid points for PM calculations, the opening angle for the tree method was 0.3 from initial to $z = 10$, and 0.5 from $z = 10$ to $z = 0$.

The calculation time was ∼180 seconds per step with 1024 cpu cores for the largest run on the Cray XT4 in Japan and ∼140 seconds per step with 2048 cpu cores on the IBM pSeries 575 in the Netherlands. We spent about 3.5 million CPU hours to perform all the 60283 steps in our simulation.

The method of identifying halos and subhalos is the same as that described in Ishiyama et al. (2009b), which is based on the spherical overdensity (Lacey & Cole 1994). The mass of the most massive halo is $5.24 \times 10^{13} M_\odot$. It contains 4.08×10^8 particles. Via Lactea I, II (Diemand et al. 2007, 2008), and Aquarius simulations (Springel et al. 2008) used $\sim 10^8$ million $\sim 5 \times 10^8$, and $\sim 10^9$ particles for the largest single halos. Table 2 shows the properties of the three most massive halos in our simulation. The virial radius of a halo is defined as the radius in which the spherical overdensity is $\Delta(z)$ times the critical value. The overdensity $\Delta(z)$ is given by the analytic formula (Bryan & Norman 1998),

$$\Delta(z) = (18\pi^2 + 82x - 39x^2)/\Omega(z), \qquad (1)$$

where $x \equiv \Omega(z) - 1$. The mass of a halo is defined as interior mass within the virial radius.

Figure 1 shows the snapshots at $z = 0$. In Figure 2, we also present the time evolution of the whole box and that of the most massive halo. The three most massive halos in simulations with three different resolutions are shown in Figure 3. The positions of subhalos agree very well in three simulations. Of course, there are some discrepancies near the centers of halos. In particular, whereas there is only one core in the center of the second massive halo (GP2) of CG2048, there are two cores in GP2 of CG1024 and CG512.

The reason of this difference is that the formation history of this halo is rather violent. It experienced many mergers near $z = 0$ in the center of the halo and is far from the relaxed state. The difference of the accuracy of integration changed the timescale of the mergers of the halos with three different resolutions. At $z = 0$, the halo GP2 has just completed the merger in the CG2048 run, whereas the same merger event is still on-going in CG1024 and CG512 runs. If we consider the spherically averaged density profile of the halo, the difference becomes important (see Section 3.2).

3. RESULTS

3.1. *Mass Function*

Press & Schechter (1974) established a recipe to derive the number of dark matter halos based on the hierarchical clustering model. Since then, a number of analytic formulae for the mass function have been proposed. Many of them are designed to give a good agreement with results of high-resolution N-body sim-

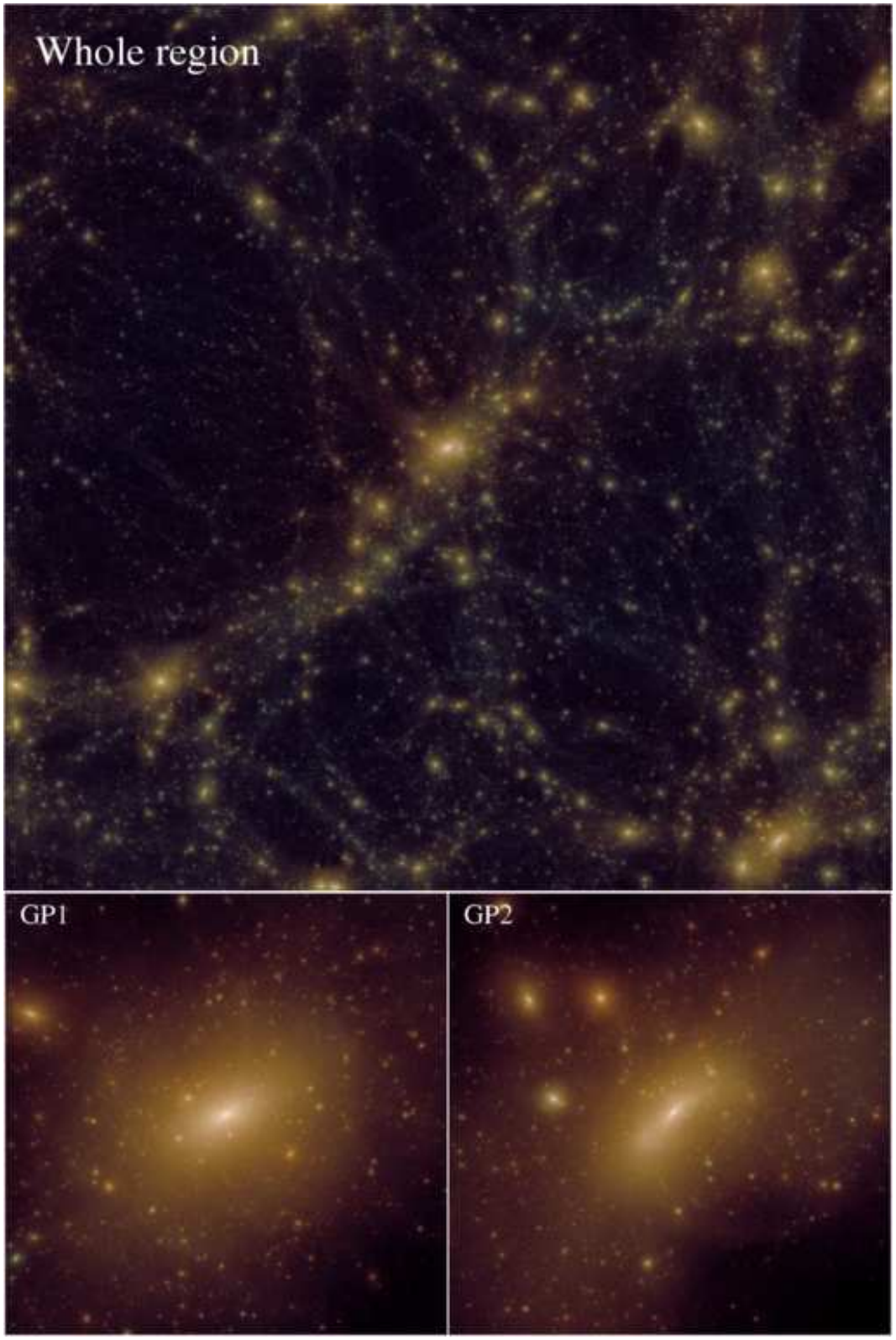

Figure 1. The projected density of dark matter at $z = 0$ in our largest simulation (2048^3 particles). Top panel shows the whole region with the volume of $(30\mathrm{Mpc})^3$. Bottom panels show the projected density of the two most massive group sized halos. These volumes are $(2\mathrm{Mpc})^3$.

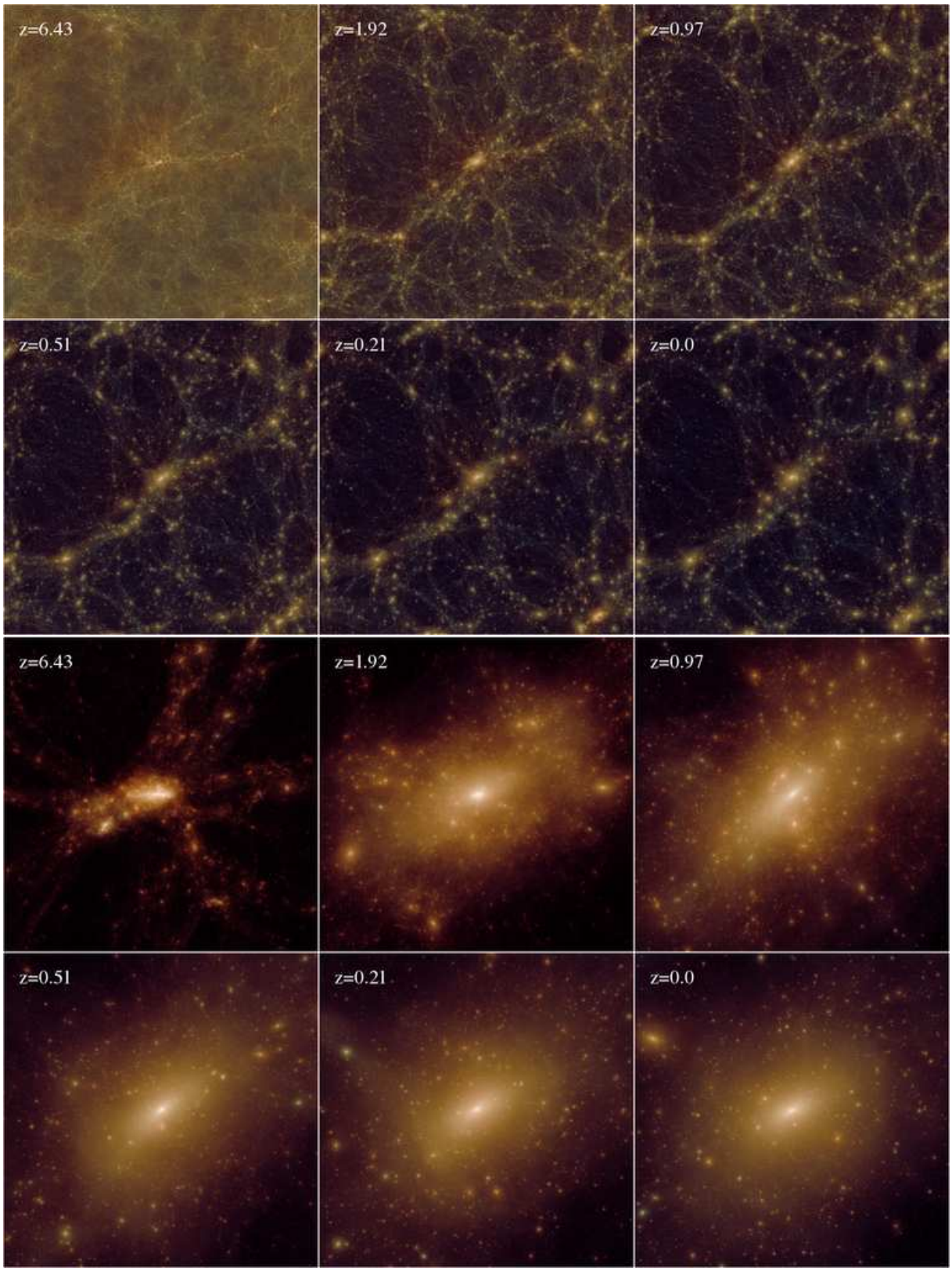

Figure 2. The evolution pictures of our largest simulation. Top six panels show the evolution of the whole region. Bottom six panels show the evolution of the most massive halo.

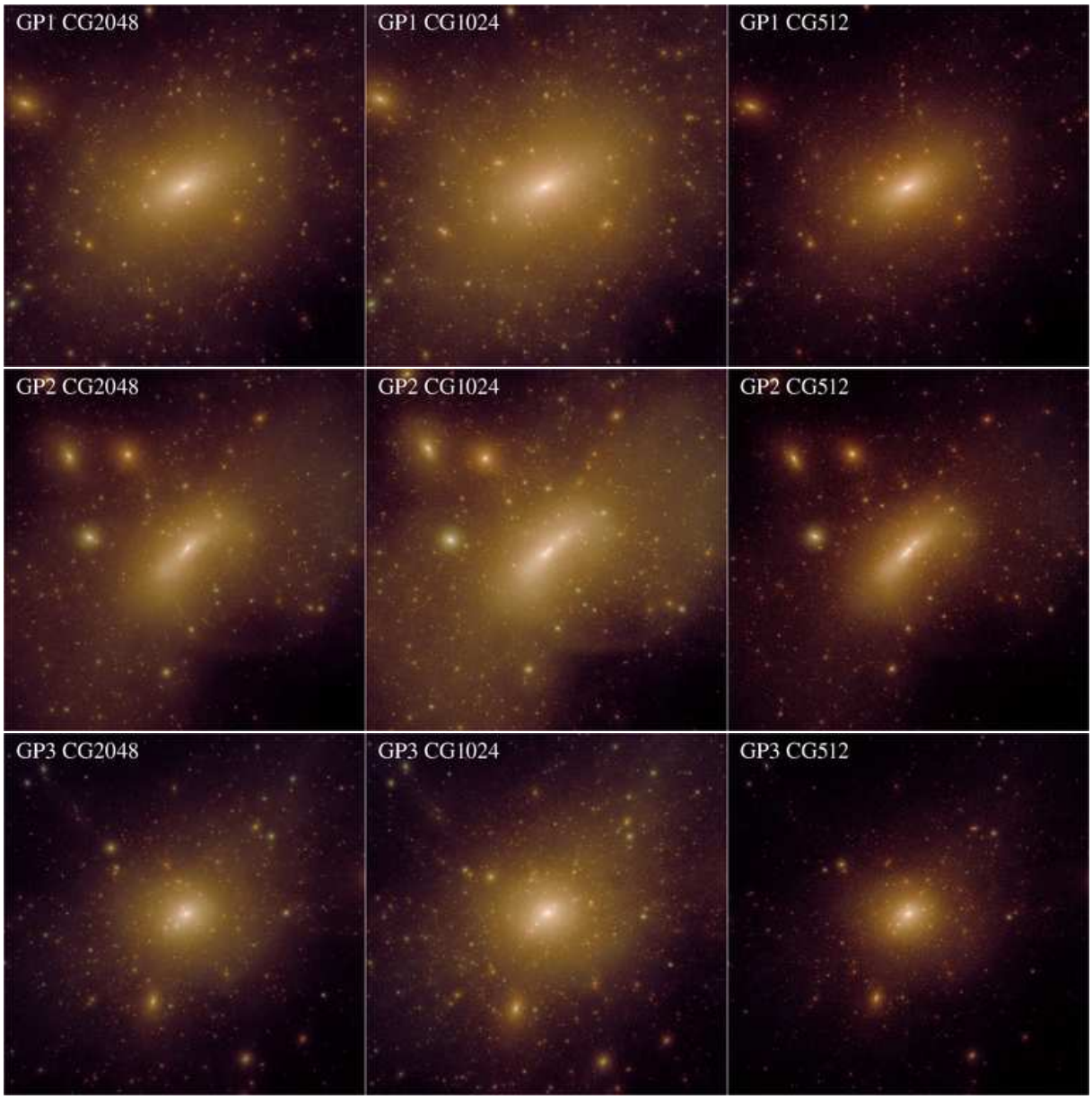

Figure 3. The projected density of dark matter at $z = 0$. Each row shows one of the three most massive halos with mass decreasing from top to bottom. Columns show different resolution from highest (left) to lowest (right).

ulations (e.g. Sheth & Tormen 1999; Jenkins et al. 2001; Reed et al. 2003; Yahagi et al. 2004; Warren et al. 2006; Tinker et al. 2008, and references therein).

These formulae can reproduce the mass function between $10^{10}M_\odot$ and cluster scale very well. Here, we examine the mass function of mass below $10^{10}M_\odot$ down to $10^7M_\odot$. The mass function of this range has been studied only in high redshift (e.g. Reed et al. 2007; Lukić et al. 2007).

Figure 4 shows the halo mass functions at three different redshifts for CG2048 run and the prediction of Sheth & Tormen formula (ST, Sheth & Tormen 1999). The agreement is very good for the mass from $\sim 10^7M_\odot$ to $M = 1.0 \times 10^{13}M_\odot$ at $z = 0$. The difference is less than 10% for $M = 5.0 \times 10^7M_\odot$ to $M = 2.0 \times 10^{12}M_\odot$ at $z = 0$, $M = 5.0 \times 10^7M_\odot$ to $M = 5.0 \times 10^{10}M_\odot$ at $z = 3$, and $M = 8.0 \times 10^7M_\odot$ to $M = 4.0 \times 10^9M_\odot$ at $z = 5.4$.

Clearly, the difference becomes larger for small mass limit as the redshift increases. This might be caused by the softening length we used. The virial radius of halos becomes smaller as the redshift increases. In other words, the ratio $R_{\rm vir}/\varepsilon$ is smaller for high redshifts. Thus, the more redshifts increase, the more the softening may reduce the number of small halos.

Our results imply that the mass function is well represented by the ST function down to $10^7M_\odot$. However, our simulations have a slightly larger number of halos than the number predicted by the ST formula. Note that the finite volume of our simulation (the box length is 30Mpc) might affect the mass function in some degrees. The absence of long wavelength perturbations might increase the number of intermediate mass halos by about 10% (Bagla & Prasad 2006; Power & Knebe 2006).

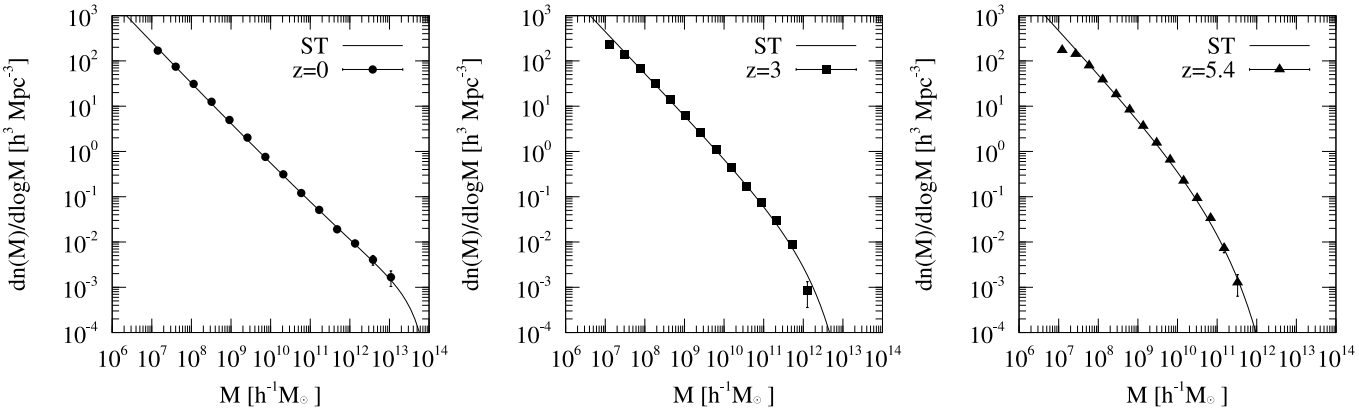

Figure 4. The mass function of our largest simulation (CG2048). The results of $z = 0.0$ (left), $z = 3.0$ (middle), and $z = 5.4$ (right) are shown. Solid curves are the Sheth & Tormen (1999) function. Error bars are Poisson errors.

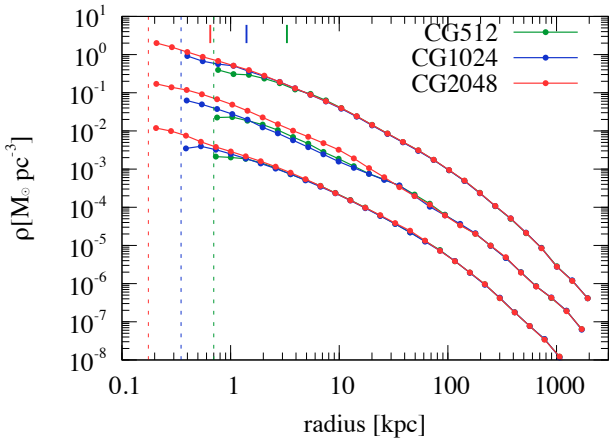

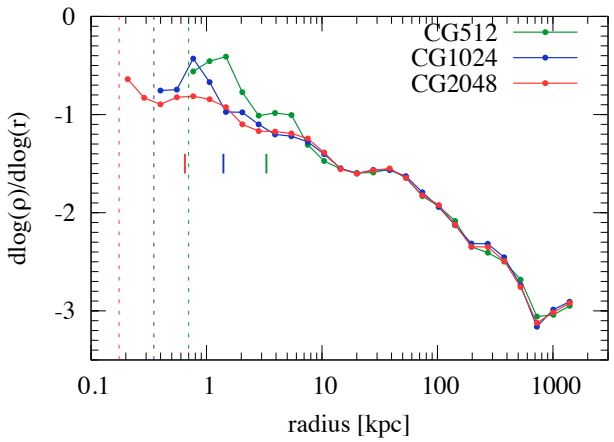

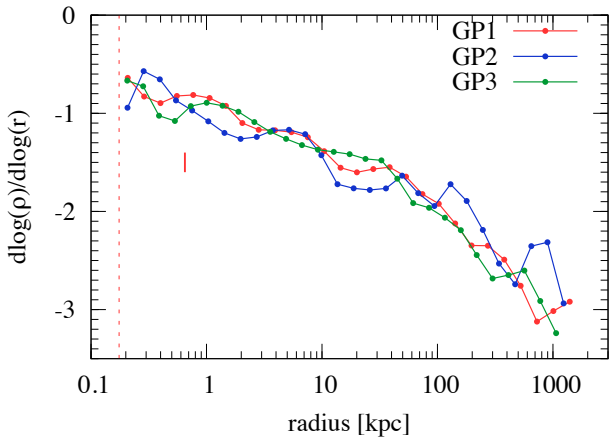

Figure 5. Spherically averaged radial density profiles of largest three halos at $z = 0$. Two of three profiles (middle and bottom) are vertically shifted downward by 1 and 2 dex. Vertical dashed lines show the softening length of three simulations. Upside short vertical bars indicate the reliability limit of the most massive halo calculated using criterion proposed by Fukushige & Makino (2001) and Power et al. (2003). The red, blue, and green correspond to the simulation CG2048, CG1024, and CG512.

Figure 6. Slopes of radial density profiles of largest three halos at $z = 0$. Top panel shows those of the largest halo for three different resolution. Bottom panel shows those of largest three halos for the largest simulation (CG2048).

3.2. *Density Structures of Most Massive Halos*

Many groups have studied the density profile of dark matter halos using high-resolution cosmological N-body simulations (e.g. Navarro et al. 1997; Fukushige & Makino 1997; Moore et al. 1999b; Ghigna et al. 2000; Jing & Suto 2000; Jing 2000; Fukushige & Makino 2001; Klypin et al. 2001; Taylor & Navarro 2001; Jing & Suto 2002; Power et al. 2003; Fukushige & Makino 2003; Fukushige et al. 2004; Diemand et al. 2004; Hayashi et al. 2004; Navarro et al. 2004; Diemand et al. 2005; Reed et al. 2005; Kazantzidis et al. 2006; Diemand et al. 2008; Gao et al. 2008; Stadel et al. 2009; Navarro et al. 2010). In most of recent works, the slopes of radial density profiles were around -1 in the inner region and around -3 in the outer region. The slope of density became shallower as the radius becomes smaller. Thus, the central slope is not described by any single power. Furthermore, the density profile was not universal. In other words, the slope showed a significant halo-to-halo scatter.

Recent studies (Stadel et al. 2009; Navarro et al. 2010) based on high resolution simulations of galactic halos showed that the slopes of density became less than -1 at the radius 0.001 times the virial radius of the halo. Einasto profile showed better agreement than the NFW profile (Navarro et al. 1997) which has been widely used for modeling dark matter halos because of its simplicity.

Almost all recent high-resolution simulations of single halos used galaxy-sized halos. Therefore, little is known

if these finding can be applied to halos of different masses. Here, we present the density profiles of three most massive halos in our simulation. These halos are galactic group-sized ones, with the mass of 5.24, 3.58, and 2.25 $\times 10^{13} M_\odot$. They contain 408, 279, and 176 million particles.

The top panel of Figure 5 shows the spherically averaged density profiles of these halos at $z = 0$. We can see that the results of three simulations with different resolution are indistinguishable for radii larger than the reliability limits, except for the second massive halo. We calculated the reliability limits using criterion proposed by Fukushige & Makino (2001) and Power et al. (2003). We can not ignore the effects of the local two-body relaxation for radii smaller than these limits. As can be seen in Figure 3, the slight difference of the merging epoch of the central cores caused this difference.

The slopes of density profiles become gradually shallower as the radius becomes smaller. The top panel of Figure 6 shows the slopes of density profiles of the most massive halo. As in the case of the density profile itself, the slopes also agree well with each other. The bottom panel of Figure 6 shows the slopes of the three most massive halos in CG2048 run.

The slope at $0.001R_{\rm vir}$ is $-0.9 \sim -1.0$ for our three halos. This value is in excellent agreement with the result of Aquarius simulation (Springel et al. 2008) or GHALO simulation (Stadel et al. 2009). Both of them gave the slope -1.0 for $r = 0.001r_{200}$. this agreement does not mean the density profile obtained by these simulation and those by our simulation are identical. The concentration parameter, which we define here as $c_{\rm vmax} = R_{\rm vir}/R_{\rm vmax}$ is 4.8, where $R_{\rm vir}$ and $R_{\rm vmax}$ are the halo virial radius and the radius of the maximum rotational velocity. This value is significantly smaller than that of Aquarius A-1 halo. Thus, the Aquarius halo is significantly more centrally concentrated, and yet the slope at $r = 0.001R_{\rm vir}$ is the same. Thus the rate of the shallowing of the slope is somewhat faster for the Aquarius halo than for our CG2048 halos. Most likely, this difference is due to the difference in the mass of the halo.

In the Cosmogrid simulation, there are 8 halos with more than 100 million particles, and 54 halos with more than 10 million particles. We will analyze the density profiles of these halos to study the dependence on the mass and other parameters.

3.3. *Concentration Distributions*

The concentration parameter has been widely used to describe the internal structure of halos since it is tightly correlated with the formation epoch (Wechsler et al. 2002). Usually, the concentration is parameterized assuming that the density profiles of halos can be fitted by the NFW profile (Navarro et al. 1997),

$$\rho(r) = \frac{\rho_0}{(r/r_{\rm s})(1 + r/r_{\rm s})^2}, \qquad (2)$$

where ρ_0 is a characteristic density and r_s is a scale radius. The concentration $c_{\rm NFW} = R/r_s$ is widely used (e.g. Bullock et al. 2001b; Zhao et al. 2003; Macciò et al. 2007; Neto et al. 2007; Macciò et al. 2008; Zhao et al. 2009; Muñoz-Cuartas et al. 2010). It is known that $c_{\rm NFW}$ depends weakly on the halo mass. Halos with higher mass have smaller concentration, since the average density of a halo reflects the cosmic density at its formation time. The dependence is weaker for higher redshift (Zhao et al. 2003).

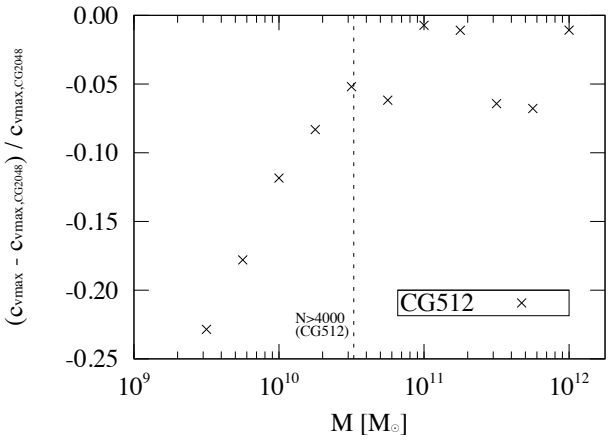

Figure 7. Residuals of concentration $c_{\rm vmax} = R_{\rm vir}/R_{\rm vmax}$ from the largest simulation (CG2048) to the lower resolution simulation (CG512).

The concentration based on the NFW profile is affected by fitting ranges and resolution (Neto et al. 2007). Furthermore, recent high resolution simulations showed that the density profile is significantly different from the NFW profile (Stadel et al. 2009; Navarro et al. 2010, also see Section 3.2). Thus, the use of $c_{\rm nfw}$ might cause some systematic bias (Gao et al. 2008; Reed et al. 2010).

We use the concentration $c_{\rm vmax}$ defined in Section 3.2, which is a simpler quantity to measure the concentration. Note that $R_{\rm vmax}$ can be easily determined directly from spherically averaged mass distribution without the need of any fitting formulae. If the density profile is represented by the NFW profile, either concentration can be converted to the other.

First, we determine the minimum number of particles in a halo necessary to reliably determine the concentration. Figure 7 shows the normalized difference of average concentration between the G2048 run and the CG512 run as the function of halo mass. We can see that the difference is ~ 0.05 for the halo mass larger than $3.0 \times 10^{10} M_\odot$. For halo mass less than $3.0 \times 10^{10} M_\odot$, the difference is larger. In the CG512 run, a halo of mass $3.0 \times 10^{10} M_\odot$ contains ~ 4000 particles. So we conclude that we need ~ 4000 particles to reliably determine the concentration. For the CG2048 run, the reliability limit is $5.0 \times 10^8 M_\odot$.

Figure 8 shows the median, and first and third quantiles of the concentration as a function of the virial mass of the halo. We can see a clear correlation between the halo mass and the concentration. Apparently, the dependence is weaker for smaller mass. Therefore, the fitting functions with a single power (e.g. Bullock et al. 2001a; Neto et al. 2007; Macciò et al. 2007; Klypin et al. 2010) cannot be used for halos of the size of dwarf galaxies.

Theoretically, the concentration of a halo reflects the cosmic density at the formation time of the halo (Bullock et al. 2001a). The concentrations of halos formed earlier are higher than that of halos formed later. However, the dependence should be weak for small halos

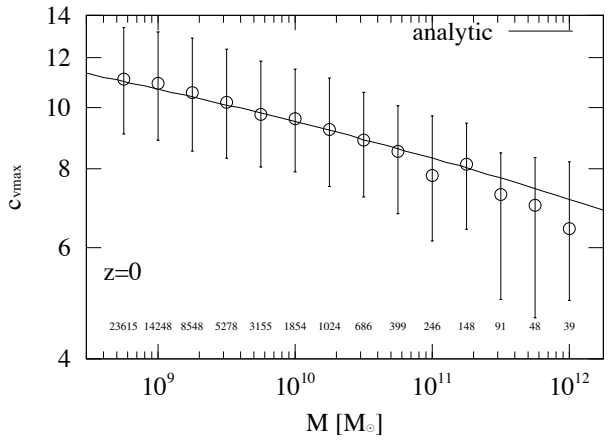

Figure 8. Concentration plotted against the halo virial mass M at $z = 0$. Circles show the median value on each bin. Whiskers are the first and third quantiles. The number of halos on each bin are shown below circles. Thick solid line shows the result from an analytical model.

since the dependence of the formation epoch to the halo mass is small for small (smaller than $10^8 M_\odot$) halos. The slope of the power spectrum of initial density fluctuations approaches to -3 for small mass limit.

In Figure 8, we also plot an analytical prediction of the mass-concentration relation, obtained by the method used in Navarro et al. (1997) assuming that all halos have the NFW profile. The formation redshift $z_{\rm f}$ of halos with the mass M is defined as the epoch at which progenitors with the mass larger than fM first contained the half of the mass M. It is estimated by using the Press Schechter formalism (e.g. Lacey & Cole 1993),

$$\mathrm{erfc}\left\{\frac{\delta_{\rm crit}(z_{\rm f})-\delta_{\rm crit}(0)}{\sqrt{2\left[\sigma_0^2(fM)-\sigma_0^2(M)\right]}}\right\}=\frac{1}{2}, \qquad (3)$$

where $\delta_{\rm crit}(z)$ is the critical overdensity for the spherical collapse at $z_{\rm f}$, and $\sigma_0^2(M)$ is the variance of the density fluctuation at $z = 0$ smoothed by a top-hat filter on a mass scale of M. Here, we used $f = 0.01$. The characteristic density ρ_0 of a halo should reflect the cosmic density at the formation time. Thus, we assume

$$\rho_0 = \rho_{\rm norm}\left(1+z_{\rm f}\right)^3, \qquad (4)$$

where $\rho_{\rm norm}$ is chosen to fit the simulation results. The mass of a halo with the NFW profile is given by

$$M = 4\pi\rho_0 r_{\rm s}^3\left[\ln(1+c)-c/(1+c)\right]. \qquad (5)$$

The mass and concentration at $z = 0$ are related to each other by

$$M=\frac{4}{3}\pi R_{\rm vir}^3\Delta(0)\rho_{\rm crit}=\frac{4}{3}\pi r_{\rm s}^3 c^3\Delta(0)\rho_{\rm crit}, \qquad (6)$$

where $\rho_{\rm crit}$ is the critical density. From equations (1), (3), (4), (5), and (6), we can analytically estimate the concentration of halos with the mass M.

As mentioned by Lacey & Cole (1993), the estimated formation epoch obtained using equation (3) is not necessarily correct. Nevertheless, as seen in Figure 8, the analytical prediction based on equation (3) shows a very good agreement with the result from CG2048 run for

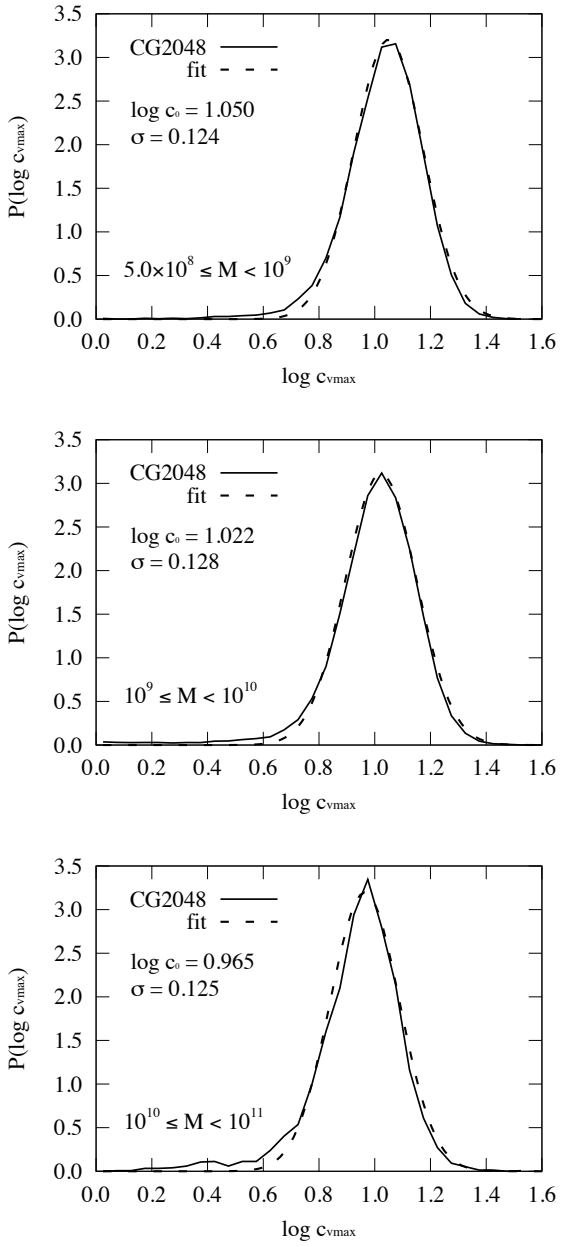

Figure 9. The probability distribution functions of the concentration at $z = 0$. These panels show the results of different mass ranges. Dashed curves are the best fits of the log-normal distribution.

halos with mass smaller than $10^{11} M_\odot$. For halos with the mass larger than $10^{11} M_\odot$, the difference between CG2048 results and analytical ones are relatively large. However, these halos are rare objects in CG2048 run, and the fact might affect the results in some degrees. We can conclude that the shallowing slope of the mass-concentration relation naturally emerges from the nature of the power spectrum of initial density fluctuations.

The slope is slightly shallower than that of $c_{\rm NFW}$ for larger halos. For the case of $c_{\rm NFW}$, the slope is around -0.10 for relaxed halos and -0.11 for all halos (Neto et al. 2007; Macciò et al. 2007). On the other hand, for the CG2048 simulation, the slope is around -0.07 for halos with the mass $10^{10} M_\odot$, and -0.06 for

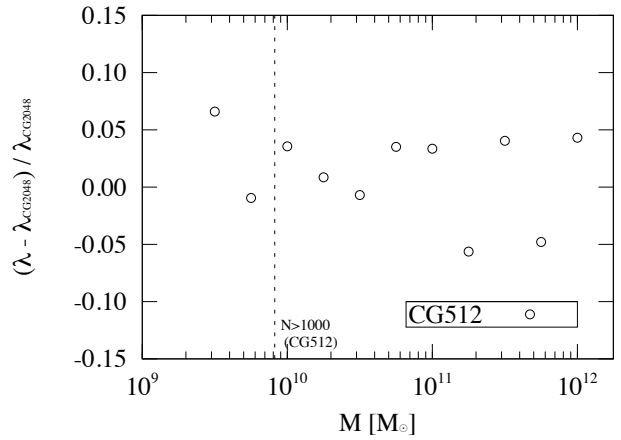

Figure 10. Residuals of spin from the largest simulation (CG2048) to lower resolution simulation (CG512).

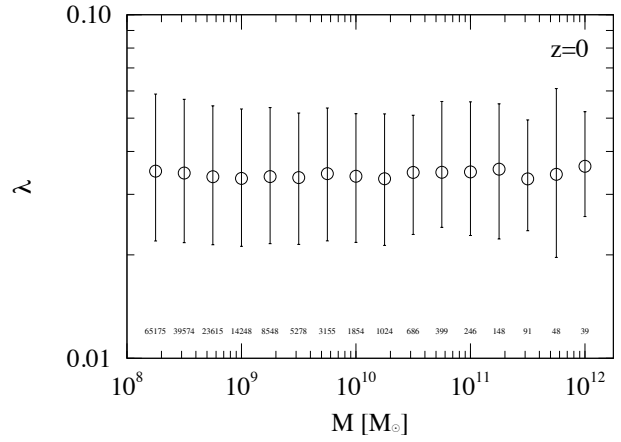

Figure 11. Spin parameter λ plotted against the halo virial mass M at $z = 0$. Circles show the median value on each bin. Whiskers are the first and third quantiles. The number of halos on each bin are shown below circles.

halos with the mass $10^9 M_\odot$. Note that one overestimates the central density of halos if one estimates the concentration of dwarf-sized halos by extrapolating the mass-concentration relation of galaxy or cluster-sized halos.

Figure 9 shows the probability distribution functions of the concentration parameter at $z = 0$ in two different mass ranges. Both shapes are well fitted by the log-normal distributions,

$$P(\log c_{\rm vmax}) = \frac{1}{\sqrt{2\pi}\sigma} \exp\left(-\frac{\log^2(c_{\rm vmax}/c_0)}{2\sigma^2}\right). \quad (7)$$

We find $\log c_0 = 1.050, \sigma = 0.124$ for halos with the mass of $5.0 \times 10^8 M_\odot \le M < 10^9 M_\odot$, $\log c_0 = 1.022, \sigma = 0.128$ for halos with the mass of $10^9 M_\odot \le M < 10^{10} M_\odot$, and $\log c_0 = 0.965, \sigma = 0.125$ for halos with the mass of $10^{10} M_\odot \le M < 10^{11} M_\odot$.

3.4. *Spin Distributions*

The dimensionless spin parameter is a good parameter to quantify the rotation of a halo. One often uses the spin parameter defined in Bullock et al. (2001a),

$$\lambda = \frac{J}{\sqrt{2} M V R}, \quad (8)$$

where M, R, V, and J is the virial mass of the halo, radius, rotational velocity at R, and total angular momentum inside R.

The distribution, the dependence on the halo mass, and the evolution have been studied by a number of works (e.g. Bullock et al. 2001a; Bailin & Steinmetz 2005; Bett et al. 2007; Macciò et al. 2007; Knebe & Power 2008; Macciò et al. 2008; Antonuccio-Delogu et al. 2010; Muñoz-Cuartas et al. 2010; Wang et al. 2010). The spin of galaxy sized halos are well studied by using the results of sufficient resolution simulations. However, we do not understand those of dwarf galaxy sized halos. The spin distribution of those halos at only high redshifts are studied by the result of high resolution simulation (Knebe & Power 2008). Here, we extend the spin distributions at $z = 0$ to dwarf galaxy sized halos (down to $10^8 M_\odot$) in the same way as the concentration.

First, we determine the minimum number of particles in a halo necessary to reliably determine the spin as done for the concentration. Figure 10 shows the normalized difference of average spin between the CG2048 run and the CG512 run as a function of halo mass. We can see that the difference is ~ 0.05 for halo mass larger than $8.0 \times 10^9 M_\odot$. For halo mass less than $8.0 \times 10^9 M_\odot$, the difference is large. In the CG512 run, a halo of mass $8.0 \times 10^9 M_\odot$ contains ~ 1000 particles. So we conclude that we need ~ 1000 particles to reliably determine the concentration. For the CG2048 run, the reliability limit is $1.28 \times 10^8 M_\odot$.

Figure 11 shows the median, and first third quantiles of the spin parameter as a function of the virial mass of the halo. Apparently, we can see the spin parameter is independent of the mass down to $10^8 M_\odot$ as pointed out for larger halos in previous works (Macciò et al. 2007; Muñoz-Cuartas et al. 2010). The median value is 0.0336.

Figure 12 shows the probability distribution functions of the spin parameter at $z = 0$ in two different mass ranges. Both distributions are almost identical. The distributions are well fitted by the log-normal distributions,

$$P(\log \lambda) = \frac{1}{\sqrt{2\pi}\sigma} \exp\left(-\frac{\log^2(\lambda/\lambda_0)}{2\sigma^2}\right). \quad (9)$$

We find $\log \lambda_0 = -1.477, \sigma = 0.308$ for halos with the mass of $1.28 \times 10^8 M_\odot \le M < 10^9 M_\odot$, $\log \lambda_0 = -1.480, \sigma = 0.288$ for halos with the mass of $10^9 M_\odot \le M < 10^{10} M_\odot$, and $\log \lambda_0 = -1.472, \sigma = 0.277$ for halos with the mass of $10^{10} M_\odot \le M < 10^{11} M_\odot$. Thus, we conclude that there is no mass dependence of the spin parameter. Otherwise, it is extremely weak.

We can see that there are small deviations from the log-normal distributions at high spin regions as seen in previous works for larger halos (Bett et al. 2007; Antonuccio-Delogu et al. 2010). If we remove unrelaxed halos, the deviations will disappear (Antonuccio-Delogu et al. 2010).

4. DISCUSSIONS AND SUMMARY

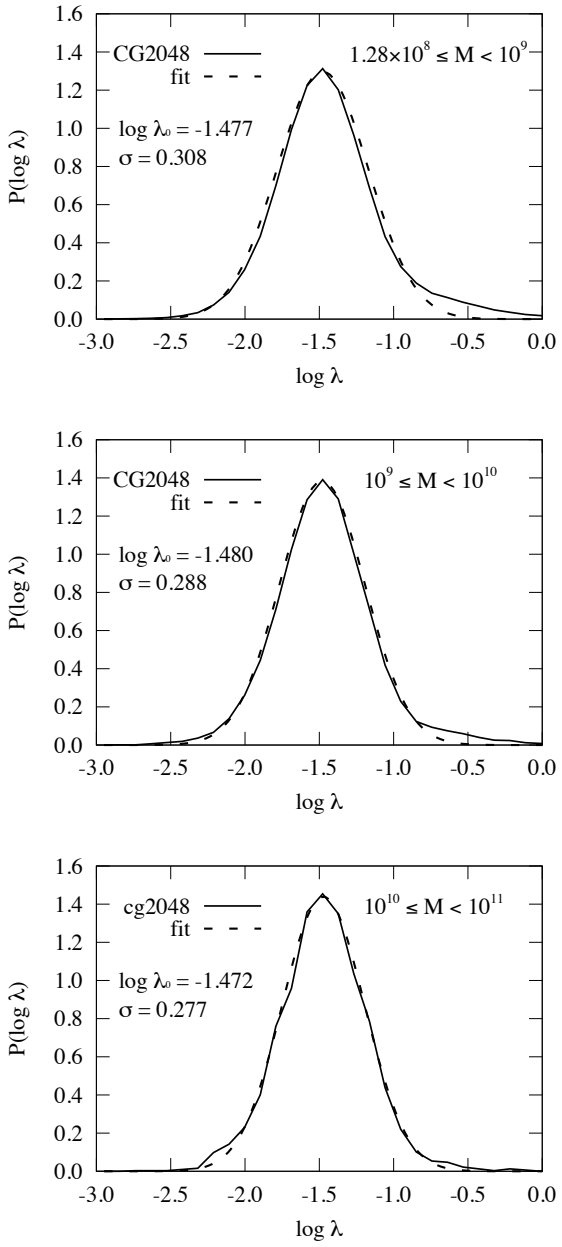

Figure 12. The probability distribution functions of the spin parameter at $z = 0$. These panels show the results of different mass ranges. Dashed curves are the best fits of the log-normal distribution.

We present the first scientific results of the Cosmogrid simulation. Because of unprecedentedly high resolution and powerful statistics, the simulation is suitable to resolve internal properties of halos with the mass larger than dwarf galaxy and subhalos whose scales are comparable to ultra-faint dwarf galaxies.

We summarize the main results of this paper as follows:

- The halo mass function is well described by the Sheth & Tormen (1999) fitting function down to $\sim 10^7 M_\odot$ from $1.0 \times 10^{13} M_\odot$. The differences are less than 10% at $z = 0$ from $M = 5.0 \times 10^7 M_\odot$ to $M = 2.0 \times 10^{12} M_\odot$.

- We analyzed the spherically averaged density profiles of the three most massive halos which contain more than 170 million particles. Their mass are 5.24, 3.58, and 2.25 $\times 10^{13} M_\odot$. We confirmed that the slopes of density profiles of these halos become shallower than -1 at the inner most radius. The results are consistent with the recent studies based on high resolution simulations for galactic halos.

- We studied internal properties of halos at $z = 0$ with the mass more than $\sim 10^8 M_\odot$. The concentration parameter measured by the maximum rotational velocity radius is weakly correlated with the halo mass. We found that the dependence of the concentration parameter with halo mass cannot be expressed by a single power law, but levels off at small mass. The slope of the mass-concentration relation is around -0.07 for halos with the mass $10^{10} M_\odot$, and -0.06 for halos with the mass $10^9 M_\odot$. The shallowing slope naturally emerges from the nature of the power spectrum of initial density fluctuations. A simple model based on the Press-Schechter theory gives reasonable agreement with the simulation result. The spin parameter does not show a correlation with the halo mass. The probability distribution functions of concentration and spin are well fitted by the log-normal distribution for halos with the mass larger than $\sim 10^8 M_\odot$.

We have shown here a first analysis of the Cosmogrid data and we plan to extend our analysis in future publications. Some of the topics that we want to address are: the variation of density profiles and its impact on the dark matter detectability, the statistics of subhalo abundance of the mass scale down to ultra faint dwarf in dwarf- and galaxy-sized halos, the assembly histories of halos, and the evolution of internal properties of halos which are presented in this paper at only $z = 0$.

Numerical computations were partially carried out on Cray XT4 at Center for Computational Astrophysics, CfCA, of National Astronomical Observatory of Japan, Huygens at the Dutch National High Performance Computing and e-Science Support Center, SARA (Netherlands), HECToR at the Edinburgh Parallel Computing Center (United Kingdom), and Louhi at IT Center for Science in Espoo (Finland). T.I. is financially supported by Research Fellowship of the Japan Society for the Promotion of Science (JSPS) for Young Scientists. This research is partially supported by the Special Coordination Fund for Promoting Science and Technology (GRAPE-DR project), Ministry of Education, Culture, Sports, Science and Technology, Japan. We also thank the network facilities of SURFnet, DEISA, IEEAF, WIDE, Northwest Gigapop and the Global Lambda Integrated FAcility (GLIF) GOLE of TransLight Cisco on National LambdaRail, Trans- Light, StarLight, NetherLight, T-LEX, Pacific and Atlantic Wave. This research is supported by the Netherlands organization for Scientific research (NWO) grant ♯639.073.803, ♯643.200.503 and ♯643.000.803, the Stichting Nationale Computerfaciliteiten (project ♯SH-095-08), NAOJ, SURFnet (GigaPort project), the International Information Science Foundation (IISF), the Netherlands Advanced School for Astronomy (NOVA), the Leids Kerkhoven-Bosscha fonds

(LKBF). We thank the DEISA Consortium (EU FP6 project RI-031513 and FP7 project RI-222919) for support within the DEISA Extreme Computing Initiative (GBBP project).

REFERENCES

Aarseth, S. J., Turner, E. L., & Gott, III, J. R. 1979, ApJ, 228, 664
Antonuccio-Delogu, V., Dobrotka, A., Becciani, U., Cielo, S., Giocoli, C., Macciò, A. V., & Romeo-Veloná, A. 2010, MNRAS, 1016
Bagla, J. S., & Prasad, J. 2006, MNRAS, 370, 993
Bailin, J., & Steinmetz, M. 2005, ApJ, 627, 647
Barnes, J., & Hut, P. 1986, Nature, 324, 446
Bertschinger, E. 2001, ApJS, 137, 1
Bett, P., Eke, V., Frenk, C. S., Jenkins, A., Helly, J., & Navarro, J. 2007, MNRAS, 376, 215
Boylan-Kolchin, M., Springel, V., White, S. D. M., & Jenkins, A. 2010, MNRAS, 406, 896
Boylan-Kolchin, M., Springel, V., White, S. D. M., Jenkins, A., & Lemson, G. 2009, MNRAS, 398, 1150
Bryan, G. L., & Norman, M. L. 1998, ApJ, 495, 80
Bullock, J. S., Dekel, A., Kolatt, T. S., Kravtsov, A. V., Klypin, A. A., Porciani, C., & Primack, J. R. 2001a, ApJ, 555, 240
Bullock, J. S., Kolatt, T. S., Sigad, Y., Somerville, R. S., Kravtsov, A. V., Klypin, A. A., Primack, J. R., & Dekel, A. 2001b, MNRAS, 321, 559
Crocce, M., Fosalba, P., Castander, F. J., & Gaztañaga, E. 2010, MNRAS, 403, 1353
Diemand, J., Kuhlen, M., & Madau, P. 2007, ApJ, 657, 262
Diemand, J., Kuhlen, M., Madau, P., Zemp, M., Moore, B., Potter, D., & Stadel, J. 2008, Nature, 454, 735
Diemand, J., Moore, B., & Stadel, J. 2004, MNRAS, 353, 624
Diemand, J., Zemp, M., Moore, B., Stadel, J., & Carollo, C. M. 2005, MNRAS, 364, 665
Efstathiou, G. 1979, MNRAS, 187, 117
Evrard, A. E., et al. 2002, ApJ, 573, 7
Fall, S. M. 1978, MNRAS, 185, 165
Fukushige, T., Kawai, A., & Makino, J. 2004, ApJ, 606, 625
Fukushige, T., & Makino, J. 1997, ApJ, 477, L9+
—. 2001, ApJ, 557, 533
—. 2003, ApJ, 588, 674
Gao, L., Navarro, J. F., Cole, S., Frenk, C. S., White, S. D. M., Springel, V., Jenkins, A., & Neto, A. F. 2008, MNRAS, 387, 536
Gao, L., White, S. D. M., Jenkins, A., Stoehr, F., & Springel, V. 2004, MNRAS, 355, 819
Ghigna, S., Moore, B., Governato, F., Lake, G., Quinn, T., & Stadel, J. 2000, ApJ, 544, 616
Groen, D., Portegies Zwart, S., Ishiyama, T., & Makino, J. 2011, ArXiv e-prints, accepted by Comp. Science and Discovery
Groen, D., Rieder, S., Grosso, P., de Laat, C., & Portegies Zwart, S. 2010, Computational Science and Discovery, 3, 015002
Hayashi, E., et al. 2004, MNRAS, 355, 794
Hockney, R. W., & Eastwood, J. W. 1981, Computer Simulation Using Particles (New York: McGraw-Hill)
Ishiyama, T., Fukushige, T., & Makino, J. 2008, PASJ, 60, L13+
—. 2009a, PASJ, 61, 1319
—. 2009b, ApJ, 696, 2115
Jenkins, A., Frenk, C. S., White, S. D. M., Colberg, J. M., Cole, S., Evrard, A. E., Couchman, H. M. P., & Yoshida, N. 2001, MNRAS, 321, 372
Jing, Y. P. 2000, ApJ, 535, 30
Jing, Y. P., & Suto, Y. 2000, ApJ, 529, L69
—. 2002, ApJ, 574, 538
Kawai, A., Makino, J., & Ebisuzaki, T. 2004, ApJS, 151, 13
Kazantzidis, S., Zentner, A. R., & Kravtsov, A. V. 2006, ApJ, 641, 647
Kim, J., Park, C., Gott, J. R., & Dubinski, J. 2009, ApJ, 701, 1547
Klypin, A., Kravtsov, A. V., Bullock, J. S., & Primack, J. R. 2001, ApJ, 554, 903
Klypin, A., Kravtsov, A. V., Valenzuela, O., & Prada, F. 1999, ApJ, 522, 82
Klypin, A., Trujillo-Gomez, S., & Primack, J. 2010, ArXiv e-prints
Knebe, A., & Power, C. 2008, ApJ, 678, 621
Komatsu, E., et al. 2009, ApJS, 180, 330
Kroupa, P., et al. 2010, A&A, 523, A32+
Lacey, C., & Cole, S. 1993, MNRAS, 262, 627
—. 1994, MNRAS, 271, 676
Li, Y., Helmi, A., De Lucia, G., & Stoehr, F. 2009, MNRAS, 397, L87
Lukić, Z., Heitmann, K., Habib, S., Bashinsky, S., & Ricker, P. M. 2007, ApJ, 671, 1160
Macciò, A. V., Dutton, A. A., & van den Bosch, F. C. 2008, MNRAS, 391, 1940
Macciò, A. V., Dutton, A. A., van den Bosch, F. C., Moore, B., Potter, D., & Stadel, J. 2007, MNRAS, 378, 55
Macciò, A. V., Kang, X., & Moore, B. 2009, ApJ, 692, L109
Makino, J. 2004, PASJ, 56, 521
Miyoshi, K., & Kihara, T. 1975, PASJ, 27, 333
Moore, B., Ghigna, S., Governato, F., Lake, G., Quinn, T., Stadel, J., & Tozzi, P. 1999a, ApJ, 524, L19
Moore, B., Quinn, T., Governato, F., Stadel, J., & Lake, G. 1999b, MNRAS, 310, 1147
Muñoz-Cuartas, J. C., Macciò, A. V., Gottlöber, S., & Dutton, A. A. 2010, MNRAS, 1685
Navarro, J. F., Frenk, C. S., & White, S. D. M. 1997, ApJ, 490, 493
Navarro, J. F., et al. 2004, MNRAS, 349, 1039
—. 2010, MNRAS, 402, 21
Neto, A. F., et al. 2007, MNRAS, 381, 1450
Okamoto, T., & Frenk, C. S. 2009, MNRAS, 399, L174
Peacock, J. A. 1999, Cosmological Physics
Portegies Zwart, S., et al. 2010, IEEE Computer, 43, 63
Power, C., & Knebe, A. 2006, MNRAS, 370, 691
Power, C., Navarro, J. F., Jenkins, A., Frenk, C. S., White, S. D. M., Springel, V., Stadel, J., & Quinn, T. 2003, MNRAS, 338, 14
Press, W. H., & Schechter, P. 1974, ApJ, 187, 425
Prunet, S., Pichon, C., Aubert, D., Pogosyan, D., Teyssier, R., & Gottloeber, S. 2008, ApJS, 178, 179
Reed, D., Gardner, J., Quinn, T., Stadel, J., Fardal, M., Lake, G., & Governato, F. 2003, MNRAS, 346, 565
Reed, D., Governato, F., Verde, L., Gardner, J., Quinn, T., Stadel, J., Merritt, D., & Lake, G. 2005, MNRAS, 357, 82
Reed, D. S., Bower, R., Frenk, C. S., Jenkins, A., & Theuns, T. 2007, MNRAS, 374, 2
Reed, D. S., Koushiappas, S. M., & Gao, L. 2010, ArXiv e-prints
Sheth, R. K., & Tormen, G. 1999, MNRAS, 308, 119
Spergel, D. N., et al. 2007, ApJS, 170, 377
Springel, V., et al. 2005, Nature, 435, 629
—. 2008, MNRAS, 391, 1685
Stadel, J., Potter, D., Moore, B., Diemand, J., Madau, P., Zemp, M., Kuhlen, M., & Quilis, V. 2009, MNRAS, 398, L21
Strigari, L. E., Bullock, J. S., Kaplinghat, M., Simon, J. D., Geha, M., Willman, B., & Walker, M. G. 2008, Nature, 454, 1096
Taylor, J. E., & Navarro, J. F. 2001, ApJ, 563, 483
Teyssier, R., et al. 2009, A&A, 497, 335
Tinker, J., Kravtsov, A. V., Klypin, A., Abazajian, K., Warren, M., Yepes, G., Gottlöber, S., & Holz, D. E. 2008, ApJ, 688, 709
van den Bosch, F. C., Tormen, G., & Giocoli, C. 2005, MNRAS, 359, 1029
Wambsganss, J., Bode, P., & Ostriker, J. P. 2004, ApJ, 606, L93
Wang, H., Mo, H. J., Jing, Y. P., Yang, X., & Wang, Y. 2010, ArXiv e-prints
Warren, M. S., Abazajian, K., Holz, D. E., & Teodoro, L. 2006, ApJ, 646, 881
Wechsler, R. H., Bullock, J. S., Primack, J. R., Kravtsov, A. V., & Dekel, A. 2002, ApJ, 568, 52
White, M., Cohn, J. D., & Smit, R. 2010, MNRAS, 408, 1818
White, S. D. M., & Rees, M. J. 1978, MNRAS, 183, 341
Yahagi, H., Nagashima, M., & Yoshii, Y. 2004, ApJ, 605, 709
Yoshikawa, K., & Fukushige, T. 2005, PASJ, 57, 849
Zentner, A. R., Berlind, A. A., Bullock, J. S., Kravtsov, A. V., & Wechsler, R. H. 2005, ApJ, 624, 505
Zhao, D. H., Jing, Y. P., Mo, H. J., & Börner, G. 2003, ApJ, 597, L9
—. 2009, ApJ, 707, 354